DuneFront

Deliverable 4.1

December 2024

DuneFront

Physical Boundary Conditions

DuneFront – D4.1

Deliverable information

Title	Physical Boundary Conditions
Deliverable number	D4.1
WP number	4
Author(s)	Bruno Castelle (UBx), Maxime Dahirel (UGent)
Lead beneficiary	UBx
Contributors	Bruno Castelle, Maxime Dahirel
Type	Report
Dissemination level	Public
How to cite	Castelle, B., Dahirel, M. (2024). Physical boundary conditions, Version 1.0, DuneFront Project Deliverable 4.1, Université de Bordeaux
Copyright license*	

Versioning and contribution history

Version	Date	Authors (Institution)	Notes
Version 0.1	28/11/2024	UBx, UGent	Version to be checked and approved by DuneFront consortium
Version 1.0	19/12/2024	UBx, UGent	Final version approved by all Beneficiaries

Funded by the European Union. Views and opinions expressed are however those of the author(s) only and do not necessarily reflect those of the European Union. Neither the European Union nor the granting authority can be held responsible for them.

Funded by the European Union

DuneFront

Cover page

The DuneFront Project is working to improve coastal protection across Europe by using Nature-based Solutions (NbS), such as Dune-Dike hybrids (DD-hybrids), to defend coastlines from extreme weather and rising sea levels. Deliverable 4.1, titled "Physical Boundary Conditions", focuses on collecting and mapping key physical boundary conditions that affect the effectiveness of these solutions. The aim is to create a consistent, high-quality dataset that helps understand how DD-hybrids are, and will be, affected by waves, tides, weather patterns, and climate change.

In order to provide useful information to the species distribution models developed in WP4.2, the study domain extends beyond the European border, covers coastlines from the Mediterranean, Black Sea, Baltic Sea, and European Atlantic, Channel, and North Sea regions, but excludes Macaronesian territories of the European Union (Canary Islands, Azores, Madeira). The dataset includes various physical boundary conditions categorized into three main groups: coastline boundaries (e.g., coastline type, orientation), hydrodynamic boundaries (e.g., wave height, tide range, storm surge), and weather conditions (e.g., temperature, precipitation, wind speed). These variables were sourced from open datasets, including satellite-derived products, numerical simulations, and global models, with detailed descriptions of each source and variable resolution provided. For future projections, the study incorporates both model-informed climate projections (CHELSA database) and linear extrapolation from recent past trends. The projections cover two periods (2041-2070 and 2071-2100) under different climate scenarios and Shared Socio-economic Pathways (SSPs). The dataset also considers interpolation techniques and addresses limitations such as the coarse resolution of wave data and potential inaccuracies in satellite-derived shoreline trends.

The study area covers 113,761 km of coastline and includes 252.5-m spaced (average) 390,240 transects. The analysis reveals significant spatial variability, with only 6.6% of the coastline consisting of sandy beaches. The proportion of sandy coasts varies widely by country, with nations like Norway contributing a large portion of the coastline but having a very low percentage of sandy beaches. In contrast, countries such as Belgium, the Netherlands, and Portugal, which have coastlines predominantly made up of sandy beaches, are considerably above the global average.

The report also highlights the variability of hydrodynamic conditions, such as wave energy, tides, and storm surges, which are crucial for understanding coastal erosion and dune dynamics. The Atlantic coast experiences high-energy wave conditions with large wave height and long wave period, whereas the Mediterranean and other enclosed seas see much lower wave height and period. The analysis of tidal conditions shows significant spatial differences, with the Severn Estuary and Bay of Mont-Saint-Michel having the highest astronomical tides

in Europe. Storm surge is notably higher along the North Sea and other regions exposed to strong winds and having wide, shallow continental shelves. The Severn Estuary, for example, experiences the highest combined tidal and storm surge levels at 11.64 m above mean sea level. Weather conditions across the European coastlines are also assessed, with data from two datasets (CHELSA and ERA5) showing a strong agreement on average air temperatures, precipitation, and cloud cover. The northern latitudes tend to have higher cloud cover and lower temperatures, while the southern Mediterranean coasts are warmer and drier. Precipitation variability is evident, with west-facing coastlines, such as those in Scotland and Norway, experiencing higher rainfall, while regions like the Mediterranean see lower precipitation levels. These patterns reflect the climatic diversity across Europe's coastlines. The report also highlights the limitations of the data mostly due to the coarse resolution of the models used to further interpolate boundary conditions along the coast, as local weather patterns (like sea breezes) are not fully captured.

The document also provides projections for future boundary conditions, using climate models to predict temperature and precipitation changes under different emission scenarios. The analysis shows that Baltic coastal regions especially are likely to experience the strongest warming, while areas such as the UK and Ireland may see less warming. Precipitation changes also vary geographically, with increased rainfall predicted for the northwestern coasts and declines in Mediterranean regions. The study emphasizes the importance of using projected climate data rather than extrapolating recent trends, due to potential mismatches between recent trends and future projections.

Despite some limitations discussed in this report, the data provides a reliable overview of the physical boundary conditions affecting the implementation and impact of DD-hybrids in Europe and beyond.

DuneFront

Table of Contents

DuneFront

List of abbreviations

Abbreviation	Explanation
WP	Work Package
DD	Dune-Dike
DD-Hybrid	Dune Dike-Hybrid
NbS	Nature based Solution
SSP	Shared Socio-economic Pathway
GCM	Global Circulation Model
CMIP6	6th Coupled Model Intercomparison Project
ECMWF	European Centre for Medium-Range Weather Forecasts
ERA5	ECMWF Reanalysis version 5
C3S	Copernicus Climate Change Services
CDS	Climate Data Store
GIS	Geographic Information System
ISO	International Standards Organization
CHELSA	Climatologies at High resolution for the Earth's Land Surface Areas
NA	Not Available

1. Introduction

1.1 Work Package 4 overview

1.1.1 General objectives

The primary objectives of Work Package (WP) 4 are to quantify and map large-scale physical, biological, and socio-economic boundary conditions that are expected to influence the effectiveness of Dune-Dike-hybrid (DD-hybrid) Nature-based Solutions (NbS). WP4 focuses on gathering and utilizing spatial information to link up morphological changes and environmental conditions (WP6), to support DuneFront's numerical modeling initiatives (WP7, WP11, WP13), physical experimental campaigns (WP12), and data-driven assessments for up-scaling efforts (WP14). This work package also aligns with Task 7.2 in another WP, which aims to collect extreme storm boundary conditions at the demonstrator level, including multiple climate change scenarios, to inform physical modeling efforts.

1.1.2 Work Package sub-tasks, milestones and deliverables

WP4 is subdivided into 3 sub-WPs listed below, each associated with a deliverable, with milestone (M4.1) involving the compilation of all boundary conditions for transfer to other WPs:

WP4.1 Physical Boundary conditions: with D4.1 (December 2024, this report) consisting in a catalogue/list/database of physical coastal boundary conditions for subsequent numerical/physical investigations.

W4.2 Distribution of important species: with D4.2 (March 2025) consisting in catalogue/list/database of the distribution of important species, providing essential data for data driven analysis and subsequent modelling.

W4.3 Socio-economic/admin boundaries: with D4.3 (October 2024) consisting in a catalogue/list/database of socio-economic and administrative boundaries for subsequent data driven analysis and upscaling analysis (Lojek et al., 2024).

1.2 Aims and objectives of D4.1

The objective of WP4.1 is to deliver consistent, high-resolution physical data—covering hydrodynamics, weather, shoreline changes, and more—at a European scale along the coast of Europe under current conditions, with extrapolations for future scenarios. To ensure data consistency across the entire European coastline, we prioritized European and global-scale datasets over combining smaller datasets from various sources, which could lead to biased or incomplete insights into European-scale physical boundary conditions.

Physical boundary conditions impacting the performance of DD-hybrid NbS can be grouped into three main categories: coastline, hydrodynamics, and weather. These datasets are

derived from various sources, primarily satellite-based shoreline data, numerical hindcasts, and projections, and are subsequently interpolated along the entire European coast. Historical trends and projections across different variables provide a foundation for new insights into future physical boundary conditions.

This report is structured as follows: Section 2 describes the study area—which extends well beyond the European border—the data sources and parameters for physical boundary conditions, as well as the methods used for interpolation and forecasting future conditions. Section 3 presents maps, close-up views, and initial statistical analyses of selected physical boundary conditions under current conditions, with a similar treatment of future scenarios in Section 4. Finally, conclusions are presented in Section 5, and a persistent DOI link to access all data products in Section 6.

2.Dataset collection and processing

2.1 Dataset overview

2.1.1 Study domain

DuneFront focuses primarily on the implementation of DD-hybrid NbS along the European Union coast. However, the species distribution models developed in WP4.2—to identify and map current and future distributions of species of conservation concern or those functionally important for coastal dune development—require physical boundary conditions that extend beyond Europe's borders. Consequently, the WP4.1 physical boundary conditions coverage has been expanded, as shown in Figure 1. The dataset covers the entire Mediterranean, Black Sea and Baltic Sea coastlines *sensu lato*, as well as the European Atlantic, Channel and North Sea coasts from Gibraltar up to the approximate latitude of the Arctic circle in Norway (matching the latitudes of the northernmost coast points in mainland EU territory, in the Baltic Sea). By contrast, Macaronesian territories of the European Union (Canary Islands, Azores, Madeira) were not included during this coverage expansion, as they are geographically and biologically distinct from the European mainland's which is the target of WP4.2 (e.g. Hernández-Cordero et al. 2015). Overall, the dataset covers 113,761 km of coastline, defined by 390,240 transects spaced on average by 251.52 m, with a minimum and maximum spacing at the highest and lowest latitude of the domain of 200 m and 431.8 m, respectively.

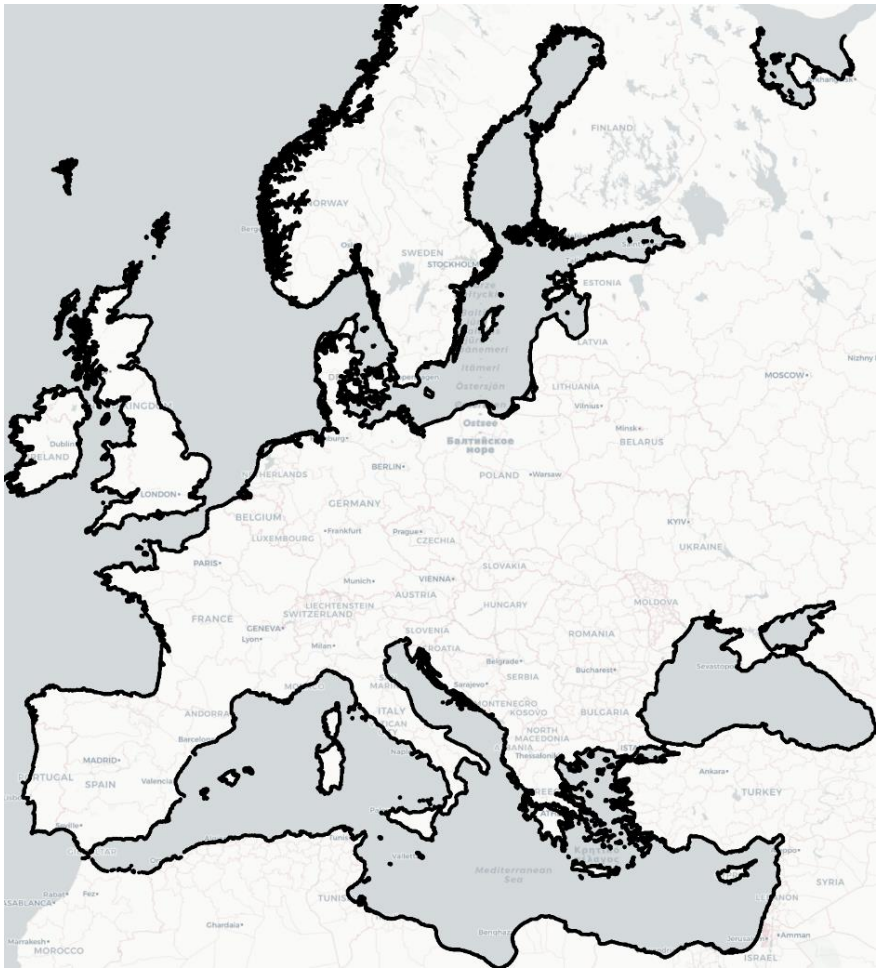

Figure 1. Coastlines (thick black line) studied here which extend beyond Europe's border

2.1.2 Datasets and physical variables

Physical boundary conditions having an expected impact on the functioning of DD-hybrid NbS can be categorized into 3 broad families:

- Coastline boundaries encompass coastal settings: coastline type *C* (0: sand, 1: mud, 2: coastal cliff, 3: vegetated, 4: other); coastline orientation β; Orthogonal distance to the closest coast *D;*
- Hydrodynamics boundaries: significant wave height *Hs;* mean wave period *T*; mean wave direction α; mean astronomical tide range *TR*; maximum astronomical tide range *HTR*; 100-year return storm surge S_{100};
- Weather boundary conditions: precipitation *P*; cloud cover *CC*; wind speed *U*; wind direction Ω; temperature *Tp*

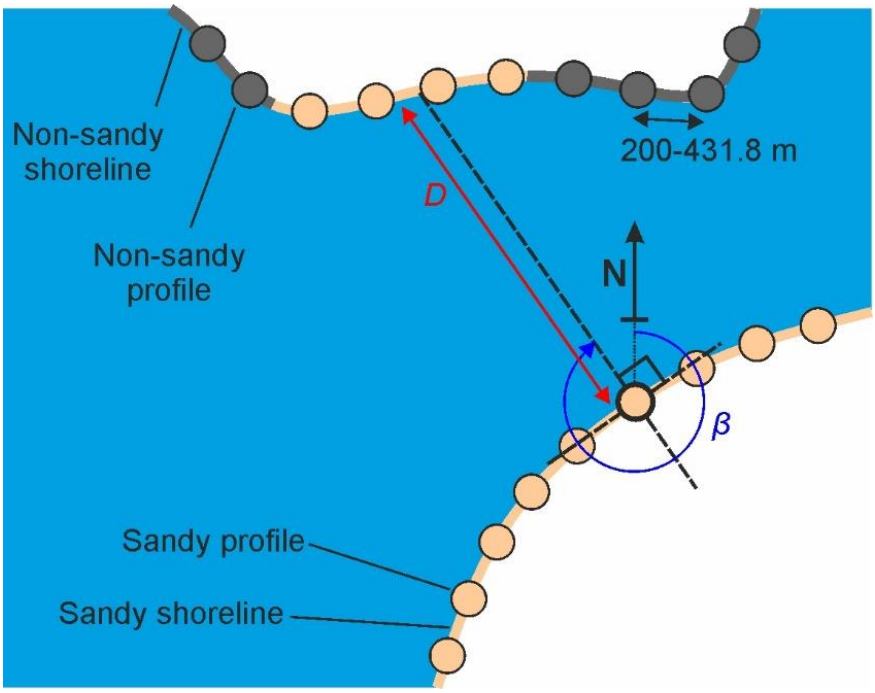

Figure 2. Coastline dataset (Luijendijk et al., 2018; Hulskamp et al., 2023) schematics and variables (modified after Castelle et al., 2024)

These variables were collected (or derived, e.g. *β*, *D*) from open datasets which are given in Table 1. Note that some weather variables were duplicated, i.e. *P* and *U,* as two different weather datasets were used (ERA5 and CHELSA, see Table 1). Coastline boundary conditions were retrieved from satellite-derived products, which were also used to collect the longitude/latitude (*Lon/Lat*) coordinates of transects covering the entire coastline. All the other variables were collected from numerical regional to global scale long-term simulations.

Table 1: List of physical boundary conditions categories and variables

Boundary condition category	**Source**	**Data access**	**Type**	**Resolution**	**Variables**
Coastline	Luijendijk et al. (2018); Hulskamp et al. (2023); Castelle et al. (2024)	Available upon request to authors	Satellite-derived shoreline transects	Transect spacing of 300-500 m	*Lat, Lon, C, β, D*
Hydrodynamics	ERA5 (Hersbach et al., 2023)	Copernicus (C3S CDS)	Numerical hindcast	0.5° grid resolution	*Hs, T, α*
	Wave indicator (Muis et al., 2022)	Copernicus (C3S CDS)			S_{100}

	TPXO Global (TPXO9_atlas_v5) (Egbert and Erofeeva, 2022)	TPXO Website https://www.tpxo.net/	Barotropic tide global model	1/30° grid resolution	*TR, HTR*
Weather	ERA5 (Hersbach et al., 2023)	Copernicus (C3S CDS)	Numerical hindcast	0.5° grid resolution	*P, CC, U, Tp, Ω*
	CHELSA version 2.1, Karger et al. (2017, 2019, 2020, 2021)	CHELSA website https://chelsa-climate.org/	Mechanistic terrain-based downscaling of global reanalysis data & global circulation models	30 sec (0.0083°) grid resolution	*P, U, Tp*

The variables are provided in several separate files for convenience (see 6 – Data availability). The definition, unit and file for each variable are further detailed in Table 2 below. Note that Table 2 also contains the variables for future projections which are addressed in Section 2.3. In total, 21 variables are provided for recent past/current conditions (not counting longitude/latitude, country, and wave/weather/water-level trends).

Table 2: List of physical boundary conditions categories and variable names and corresponding files

File name	Variable name	Unit	Description
In all files	longitude	degrees	Longitude of the midpoint of the reference transect
	latitude	degrees	Latitude of the midpoint of the reference transect
	country	NA	Country in which the reference transect is located (using midpoint longitude and latitude), based on Eurostat data for 2024 (https://ec.europa.eu/eurostat/web/gisco/geodata/administrative-units/countries, accessed 2024-11-21, © EuroGeographics). The inclusion of these reference data for informational purposes should not be construed as an endorsement by the authors, or the DuneFront consortium, of any specific territorial claim regarding disputed territories.
	country_iso	NA	Corresponding ISO 3166-1 alpha-3 code for the country
	sediment_label	NA	5 possible values: Sand, Mud, Coastal cliffs, Vegetated, other
	shoreline_trend	m/year	Long-term (1984-2021) shoreline trend from a linear regression of the yearly shoreline positions

	coastline_orientation	degrees	North-exposed coastline are 0°, positive clockwise
	distance_closest	km	Orthogonal distance to the closest shoreline (200 km limit)
DuneFront_D4.1_means	wave_height	m	Average significant Wave Height over the 1940-2023 climatological period
	wave_period	s	Average mean Wave Period over the 1940-2023 climatological period
	wave_angle	degrees	Average Wave Angle over the 1940-2023 climatological period, in nautical convention, i.e. the direction where the waves come from measured clockwise from geographic North
	tide_range	m	Mean Tide Range
	highest_astro_tide	m	Highest Astronomical Tide
	ss_100yr	m	100-year return Storm Surge estimated from the 2001-2017 climatological period
	tmp	K	Average air Temperature over the 1940-2023 climatological period
	pre	m	Average annual Precipitation over the 1940-2023 climatological period
	cloud_cover	proportion [0-1]	Average cloud Cover over the 1940-2023 climatological period
	wind_lat	m/s	Average latitudinal wind over the 1940-2023 climatological period
	wind_lon	m/s	Average longitudinal wind over the 1940-2023 climatological period
DuneFront_D4.1_trends	slope_[variable], where [variable] is the name of one of the variables exclusive to DuneFront_D4.1_means	[variable] units / year	slope of the local linear regression of monthly values of [variable] on time
	r_[variable]	NA	Pearson correlation coefficient between monthly values of [variable] and time
	p_[variable]	NA	p-value of the local regression of monthly values of [variable] and time
DuneFront_D4.1_CHELSA_means	CHELSA_tas	K	average temperature over the 1989-2018 climatological period
	CHELSA_tasmin	K	average daily minimal temperature of the coldest month of the year over the 1989-2018 climatological period
	CHELSA_tasmax	K	average daily maximal temperature of the warmest month of the year over the 1989-2018 climatological period
	CHELSA_pr	m	average total annual precipitation over the 1989-2018 climatological period

	CHELSA_sfcWind	m/s	average wind speed over the 1989-2018 climatological period
	CHELSA_sfcWind_max	m/s	average wind speed of the windiest month of the year over the 1989-2018 climatological period
DuneFront_D4.1_CHELSA_trends	slope_[CHELSA_variable], where [CHELSA_variable] is the name of one of the variables exclusive to DuneFront_D4.1_CHELSA_means	[CHELSA_variable] units / year	slope of the local linear regression of annual values of [CHELSA_variable] on time
	r_[CHELSA_variable]	NA	Pearson correlation coefficient between annual values of [CHELSA_variable] and time
	p_[CHELSA_variable]	NA	p-value of the local regression of annual values of [CHELSA_variable] on time
DuneFront_D4.1_CHELSA_projections	[CHELSA_variable]_[start]_[end]_[scenario]	[CHELSA_variable] units	average of the predictions of the 5 models included in CHELSA v2.1 for the specified [CHELSA_variable], climatological period from years [start] to [end] (inclusive) and emission [scenario]

2.2 Future projections

Two different approaches were used to address the future of physical boundary conditions along the European coast. First, climate projections over the 2041-2070 and 2071-2100 under different CMIP6 scenarios were collected from CHELSA (Section 2.2.1). However, given that these projections were only available for a limited number of variables, namely precipitation and temperature, past linear trends were also computed for both ERA5 variables (1940-2023) and CHELSA (1989-2018), which can be further extrapolated by the user for future conditions (Section 2.2.2, but see Section 4.2).

2.2.1 Climate model-informed projections (CHELSA)

In addition to recent past/current conditions data, the CHELSA database also includes ready-to-download projections of future conditions over the 2041-2070 and 2071-2100 climatological periods (see Karger et al. 2019, though they describe previous versions of the dataset; for up-to-date technical specifications, see documentation at https://chelsa-climate.org/downloads/, under version 2.1). These predictions are available for a selected number of CMIP6 scenarios, covering 3 Shared Socio-economic Pathways (SSPs) and 5 different Global Circulation Models (GCMs).

The three SSPs are (Riahi et al. 2017, IPCC 2023):

- SSP1-RCP2.6 ([scenario] "ssp126" in file names, low greenhouse gas emissions, "Sustainability – Taking the Green Road" narrative),
- SSP3-RCP7 ([scenario] "ssp370" in file names, high greenhouse gas emissions, "Regional Rivalry – A Rocky Road" narrative),
- SSP5-RCP8.5 ([scenario] "ssp585" in file names, very high greenhouse gas emissions, "Fossil-fueled Development – Taking the Highway" narrative).

The five GCMs are: GFDL-ESM4, UKESM1-0-LL, MPI-ESM1-2-HR, ISPL-CM6A-LR and MRI-ESM2-0 (Lange 2021). For each SSP, time period, and variable, we first generated raster layers averaging the predictions of the five CMIP6 GCMs. As with the present-day layers, we then sampled these layers at the locations of all transects, resulting in our final outputs (Table 2).

2.2.2 Linear extrapolation from current conditions

However, these model-informed projections are readily available only for CHELSA layers, and even then, not for all layers; there are no projections available for wind speed or wave height for instance. Users may nonetheless be interested in (i) future projections for any of the other layers, and/or (ii) predicting for a specific year/ a different time interval than those used in CHELSA "official" projections. For (ii) specifically, we note that the CHELSA authors made a Python package that gives users finer control over their choice of period, among other things; see https://gitlabext.wsl.ch/karger/chelsa_cmip6 [accessed 2024-11-12]. For both (i) and (ii), extrapolating from recent past/current linear trends may also be suitable as a first approach.

Contrary to the CHELSA-based projections, we do not include ready-made layers for these extrapolations, as different users may be interested in different layer/period combinations. We do however provide below a short reminder on how to easily obtain such layers from the current conditions layers and trends included in the deliverable.

- Let y be a variable of interest measured at regular intervals over a time period $[t-i, t+i]$, with t the average time value,
- $\bar{y}$ the average value of y over the above time period,
- and β be the slope of the linear regression of y over time.
- Then the predicted value of y for any future time $t + j$ is : $\bar{y} + \beta \times j$.
- Mean values ($\bar{y}$) and slopes (β) are the present-day layers included in this deliverable (see part 3 of this report). Values for t can be obtained from the definitions of each variable Table 2, which include $[t-i, t+i]$ (t = 1981.5 for the ERA layers, and 2003.5 for the CHELSA layers).

2.3 Interpolation and limitations

All the variables listed in Table 2, including trends and p-values, were systematically interpolated on the shoreline dataset i.e. on the 390,240 individual transects spaced on average by 251.52 m and thus covering 113,761 km of coastline. Different interpolation

techniques were used depending on the dataset. These interpolation techniques and limitations are listed in Table 3 below.

Additionally, we note that for a few variables, a limited (well below 1%) number of transects in our final dataset contain missing values, due to either blank pixels in raw data that our procedure propagated, or to mismatches between our transect and raw data (for instance, some transects located deep into fjords in our coastline dataset were mistakenly seen as inland, rather than coastal, in some of our data sources with coarser resolution). For these, we encourage readers to impute values at these locations, if needed, as they judge most appropriate for their use case. There is a wider missing values issue in wave (height, period and direction) trends layers however, again tracing back to the raw data source. Here, we recommend users do not impute missing values, but only use the transects with available data.

Table 3. Interpolation techniques and limitations

Boundary condition category	**Data source**	**Interpolation**	**Primary limitations**
Hydrodynamics	ERA5 (Hersbach et al., 2023)	Nearest (water grid cell) neighbor	The data is interpolated from a global wave model with a 0.5° grid resolution, meaning that wave transformations along the coast (such as refraction, sheltering, etc.) are not accounted for. Due to the coarse resolution, the water levels at grid points may vary significantly, which could affect the consistency of the data. Overall, the wave conditions are expected to be broadly representative of coastal wave conditions. However, for embayed and/or sheltered coasts, which account for a large portion of the coastline in this dataset, the wave conditions—particularly wave height—are likely to be inaccurate due to the influence of the dominant wave incidence. Therefore, readers are encouraged to consult regional or local wave models for more accurate wave conditions specific to their site
	Wave indicator (Muis et al., 2022)	Nearest neighbor	Interpolation from an already interpolated coastal dataset, which may induce some slight smoothing
	TPXO Global (TPXO9_atlas_v5) (Egbert and Erofeeva, 2022)	Nearest (water grid cell) neighbor	Tidal data may slightly differ locally around estuaries and bay due to tidal model resolution

Weather	ERA5 (Hersbach et al., 2023)	Linear interpolation	Given the coarse grid resolution, local weather effects (e.g. sea breeze, some catabatic winds) are not taken into account
	CHELSA version 2.1, Karger et al (2017, 2019, 2020,2021)	Nearest grid cell	The finer grid cell resolution is achieved using terrain-based downscaling of ERA data, accounting for wind effects (Karger et al., 2017). The apparent increased local precision in CHELSA is therefore fully dependent on the local performance of this downscaling procedure (see Karger et al (2017) for validation details)

Another limitation of the present dataset concerns the satellite-derived products. As acknowledged by Luijendijk et al. (2018) and Castelle et al. (2024), the uncertainties in satellite-derived shoreline trends are approximately ±0.5 m (Luijendijk et al., 2018), with a potential bias towards accretion of +0.2 m/yr (Castelle et al., 2024) and, locally, flawed long-term trends. In line with the recommendations of Castelle et al. (2024), readers are encouraged to apply moving alongshore averaging to smooth out shoreline trend outliers, and to consider large uncertainties when planning to extrapolate past change to future shoreline position.

In addition, although the new classification (Hulskamp et al., 2023) of sandy, muddy, and cliff coasts provides a better distinction between sandy and other environments (Castelle et al., 2024), some coastal sectors may still be misclassified. Quality checks conducted along specific sectors of the present dataset suggest that it is limited to a small range of coastal environments—e.g., some sandy intertidal zones are classified as muddy coasts.

3. Physical boundary conditions maps under current conditions

In this section, we provide an overview of the dataset. For brevity, only a selected number of layers (out of 21 in total, representing current and past conditions) are mapped, along with some general statistics. For a more detailed examination, readers are encouraged to explore the layers provided in the various files (Table 2) using GIS software, for example.

3.1 Coastline layers

The dataset covers 113,761 km of coastline, defined by 390,240 transects. Overall, the coastline studied here exhibits a wide range of coastal environments (see zoom in Figure 3) with significant spatial variability. Notably, only 25,770 km (6.6%) of the coastline is sandy. This low proportion is largely driven by countries like Norway, which contributes a substantial portion of the total coastline (≈18,000 km, even though it is not fully included in the dataset), but has an exceptionally low proportion of sandy beaches (≈2%). In contrast, countries such as Belgium, the Netherlands, Poland, and Portugal have coastlines where more than half consists of sandy beaches—well above the global average of approximately 31% (Luijendijk et al., 2018).

Figure 3. Zoom on coastal type showing a large spatial variability in terms of coastal environments (sand, cliff, vegetated, mud, other)

Amongst the 25,770 km of sandy coasts, according to the satellite-derived shoreline dataset approximately 13.5 % are eroding at a rate > 0.5 m/year, while a larger proportion (22.8%) is accreting, with a mean satellite-derived sandy shoreline trend of 0.28 m/yr. It is important, however, to remind that this satellite-derived shoreline product may be slightly biased towards erosion (Castelle et al., 2024) and that such trends are associated with substantial uncertainties.

3.2 Hydrodynamic layers

Incident wave conditions, astronomical tides, and storm surges are critical factors in beach and coastal dune erosion. The three figures (Figures 4, 5 and 6) below provide insights into the spatial variability of these key variables on a European scale.

Figure 4 highlights a clear distinction between the long-wave-dominated Atlantic coast of Europe, which is exposed to high-energy ocean waves generated in the North Atlantic (with average wave periods exceeding 8 seconds), and other regions, particularly along the more sheltered coastal sectors of the Mediterranean Sea, as well as the Adriatic, Black, and Baltic Seas, where the mean wave period is generally under 4 seconds. This difference is also reflected in the variability of time-averaged wave heights (not shown). Regarding wave direction (also not shown), waves consistently approach from the west-northwest along the Atlantic coast of Europe, while the angle of wave incidence shows much greater variability in the other regions.

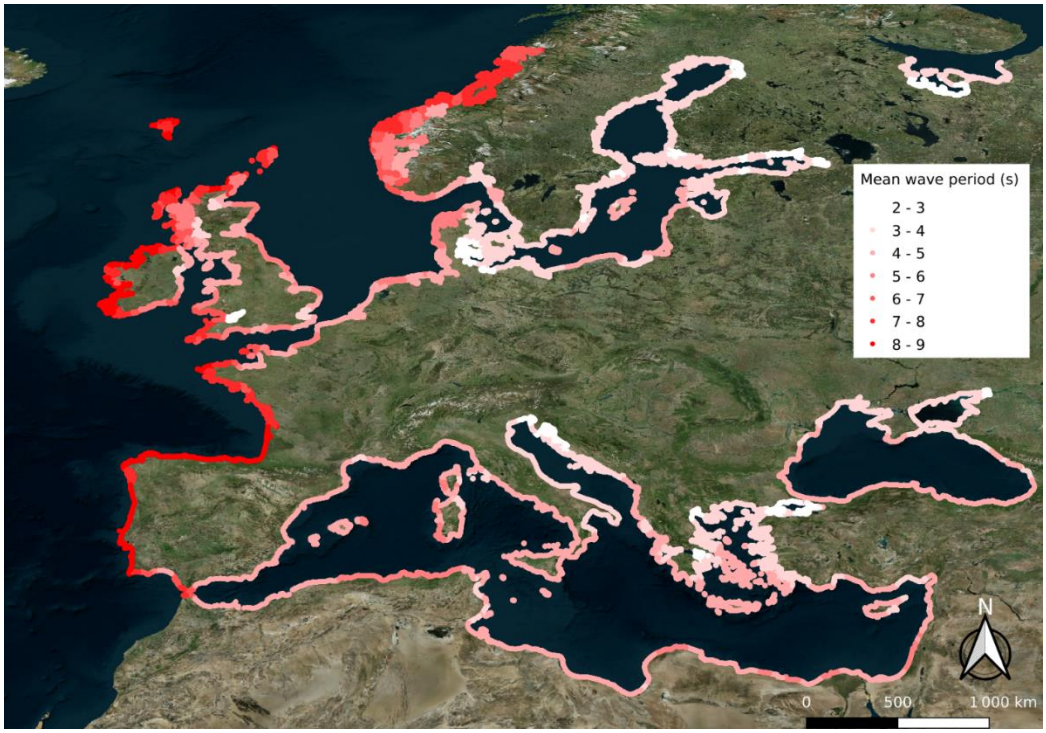

Figure 4. Map of averaged (1940-2023) mean wave period (wave_period in DuneFront_D4.1_means) in seconds.

The two following figures show the variability of coastlines in terms of potential water level, with the highest astronomical tide (Figure 5) and the 100-year return period storm surge (Figure 6). The highest tides are located in the Severn Estuary (England/Wales), peaking at 7.87 m according to TPXO, and the Bay of Mont-Saint-Michel in France, peaking at 7.85 m according to TPXO. Tides are very low in the Mediterranean Sea and in the Adriatic, Black, and Baltic Seas, while they are much more variable along the coasts of the Atlantic and North Sea. The storm surges (Figure 6), on the other hand, are typically most significant in areas that are exposed to potentially the strongest winds and are facing a wide, shallow continental shelf, which increases storm surge amplitude. This is why the largest storm surges are typically observed along the coasts of the North Sea, with an estimated 100-year return storm surge peaking at 5.84 m in the Elbe and Jade-Weser estuaries in Germany. Overall, the estimated current maximum potential water level elevation (astronomical tide + 100-year return storm surge) at the study area is 11.64 m above mean sea level in the Severn Estuary (England/Wales).

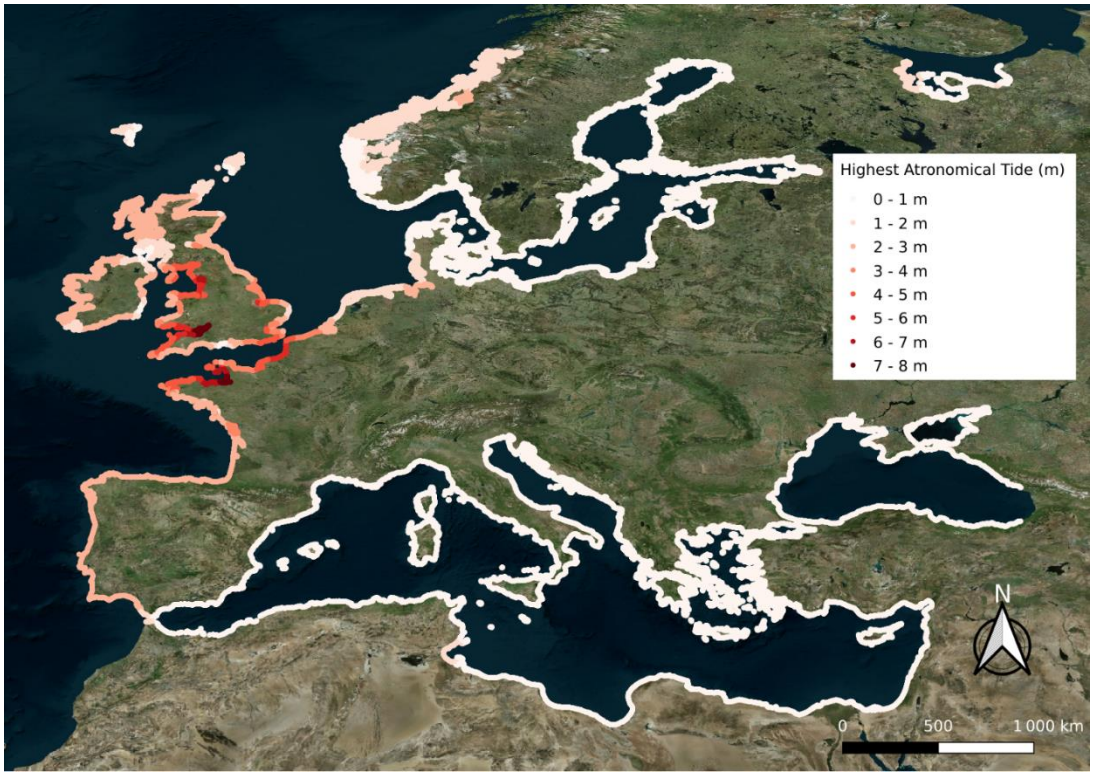

Figure 5. Map of highest astronomical tide level (highest_astro_tide in DuneFront_D4.1_means) in meters

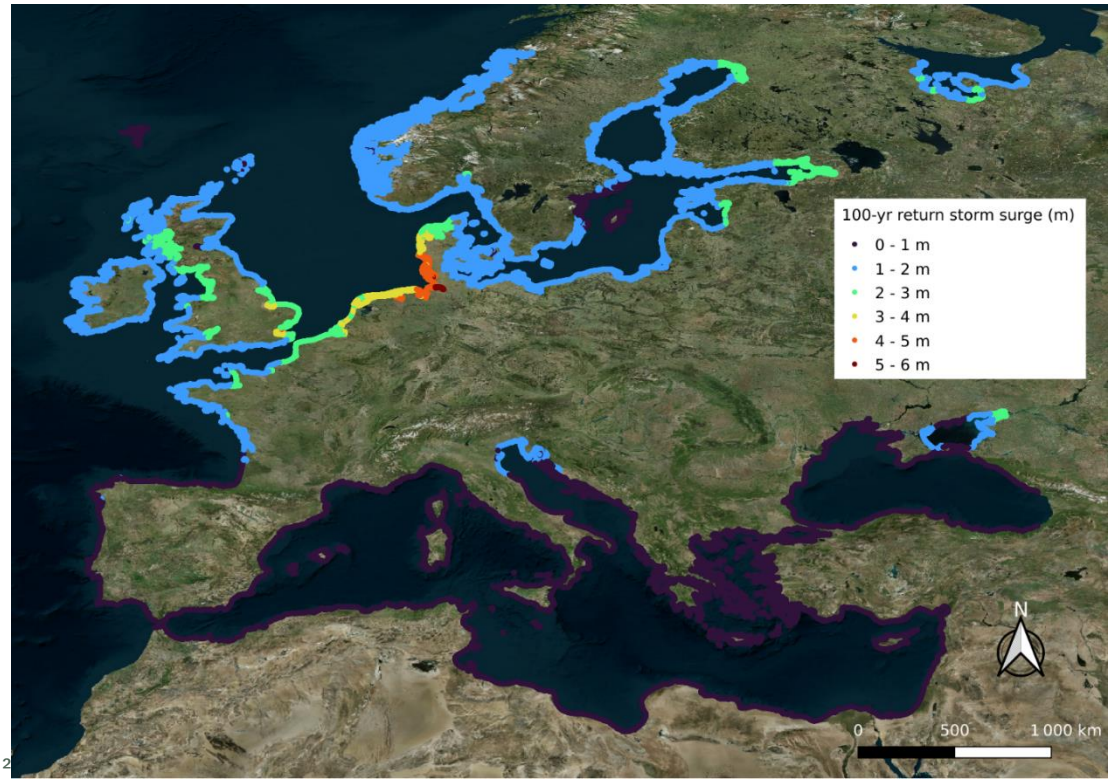

Figure 6. Map of 100-year return Storm Surge (ss_100yr in DuneFront_D4.1_means) in meters

3.3 Weather layers

In contrast to the hydrodynamic layers, some of the weather boundary conditions were available from two datasets (Table 1). Figure 7 compares the average temperatures from CHELSA and ERA, showing a strong overall agreement between the two datasets (*R2* = 0.97, RMSE = 0.81°), which supports the reliability of using either dataset. The deviation from the $x = y$ line (with CHELSA giving generally higher values) reflects the different temporal coverage of the two datasets and global warming.

Overall, all weather datasets reveal a clear latitudinal gradient. For instance, higher cloud coverage (Figure 8) and lower temperatures (Figure 9) are observed at the northernmost latitudes. Minimum cloud coverage (0.23) is recorded along the southern coast of Cyprus, while the cloudiest coastal region (0.84) is located in western Scotland. The coldest coastal area (274.45 K) is found in Russia near the White Sea, whereas the warmest coastal region (294.82 K) lies along the eastern Nile Delta in Egypt. Greater variability is observed for precipitation (Figure 10). While some latitudinal gradients persist, west-facing coastlines also tend to experience higher precipitation rates.

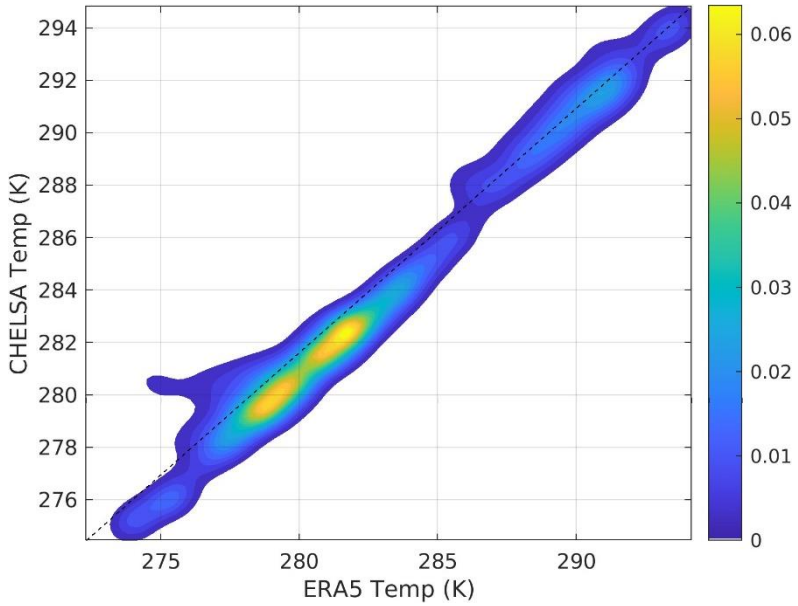

Figure 7. Smoothed density plot of CHELSA average air temperature (CHELSA_tas) and ERA5 average temperature (tmp) across the entire coastline

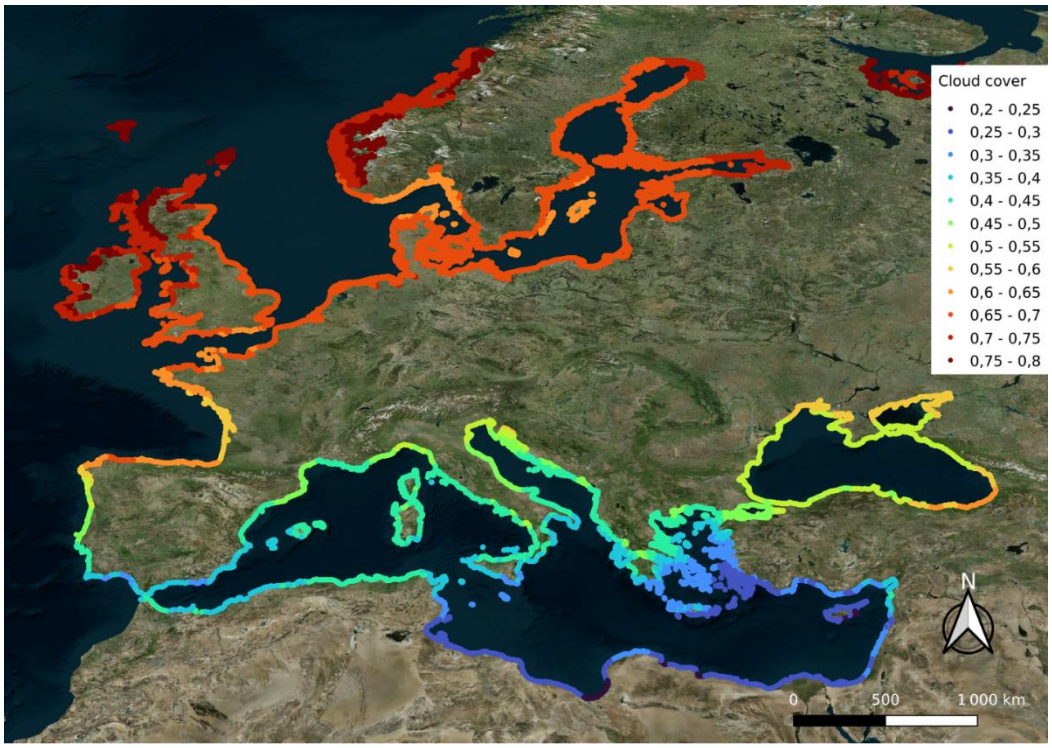

Figure 8. Map of cloud cover (cloud_cover in DuneFront_D4.1_means)

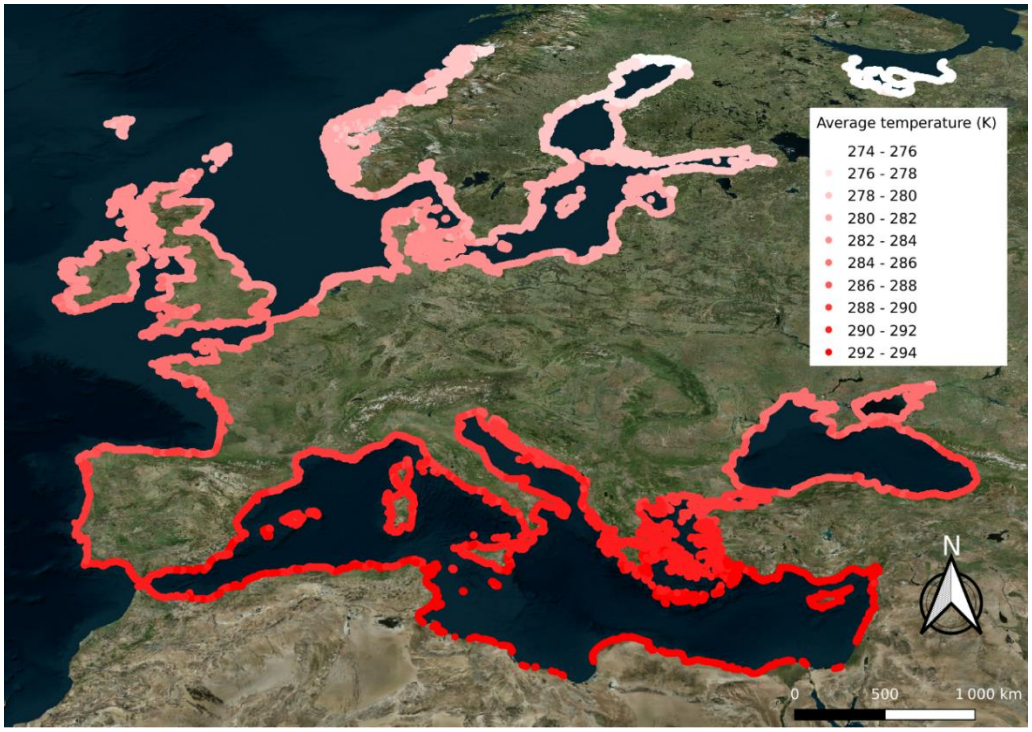

Figure 9. Map of average air temperature (CHELSA_tas in DuneFront_D4.1_CHELSA_means)

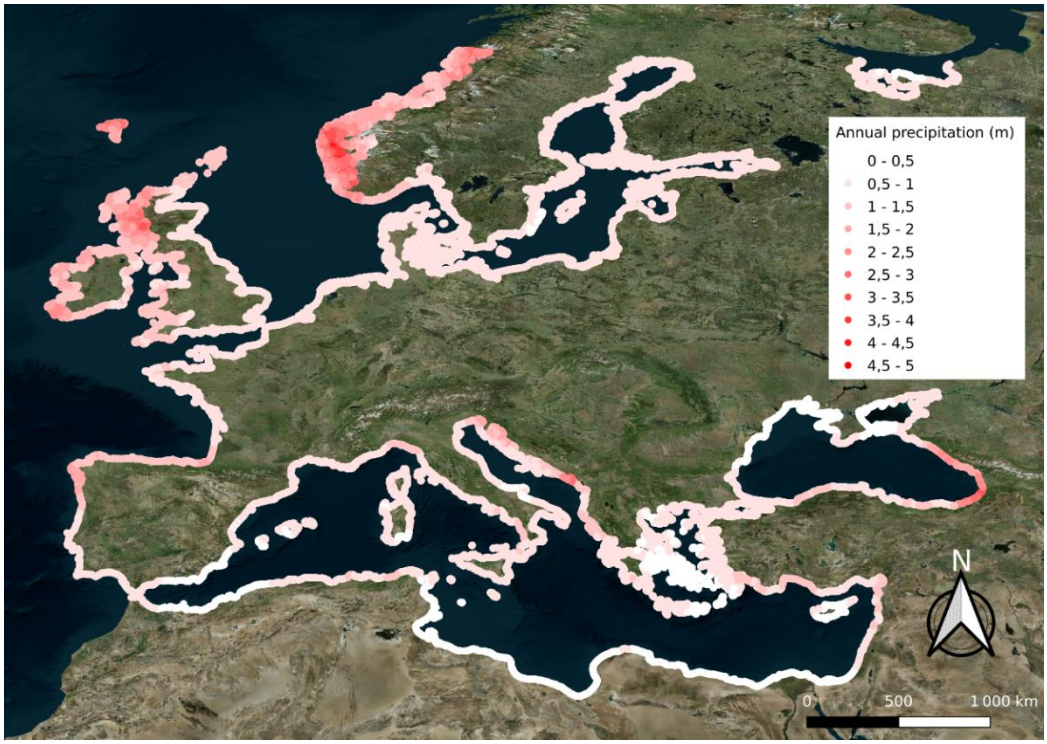

Figure 10. Map of average total annual precipitation (CHELSA_pr in DuneFront_D4.1_CHELSA_means)

4. Future projection of boundary conditions

We provide a brief overview of a few of the "future conditions" layers, along with general statistics and comparisons. For brevity, here we only focus on weather layers. As in Section 3, readers are encouraged to use e.g. GIS software to explore the layers in more detail.

4.1 Weather layers: Expected future climate under different climate scenarios (CHELSA data)

The correlations between transect-level CHELSA present (DuneFront_D4.1_CHELSA_means) and projected (DuneFront_D4.1_CHELSA_projections) temperature and precipitation values are extremely strong, irrespective of climate scenario and time horizon (Pearson's *r* values always > 0.96 and very often > 0.99). As a result, qualitative spatial patterns in future weather conditions are almost identical to those for present conditions shown Figures 8-9, and we do not redescribe them here.

Instead, we show in Figures 11 and 12 the differences between present-day (1989-2018) and near-future (2041-2070) temperatures and precipitations, using the intermediate SSP3-RCP7 ("ssp370") as an example. Figure 11 shows that the Baltic coasts are predicted to experience the strongest warming under that scenario, with expected annual temperatures over 2 Kelvin (2°C) higher than the "present". By contrast, Atlantic coasts, especially in the UK and Ireland, are expected to see the lowest levels of warming. However, we must note that in this intermediate emission and near-future scenario, there is still no transect that is predicted to experience less than a 0.7 Kelvin (0.7°C) temperature increase compared to the "present".

Figure 12 shows that spatial heterogeneities in precipitation visible in Figure 10 will increase in the near future. Indeed, the coastal regions experiencing the most precipitation in the present day (Scottish and Norwegian coasts especially) are predicted to receive even higher amounts in the near future, with increases of over 0.15 m and up to nearly 0.5 m in some cases. By contrast, many transects in the Mediterranean region, which are already among the driest of our dataset, will see further declines in precipitation rates.

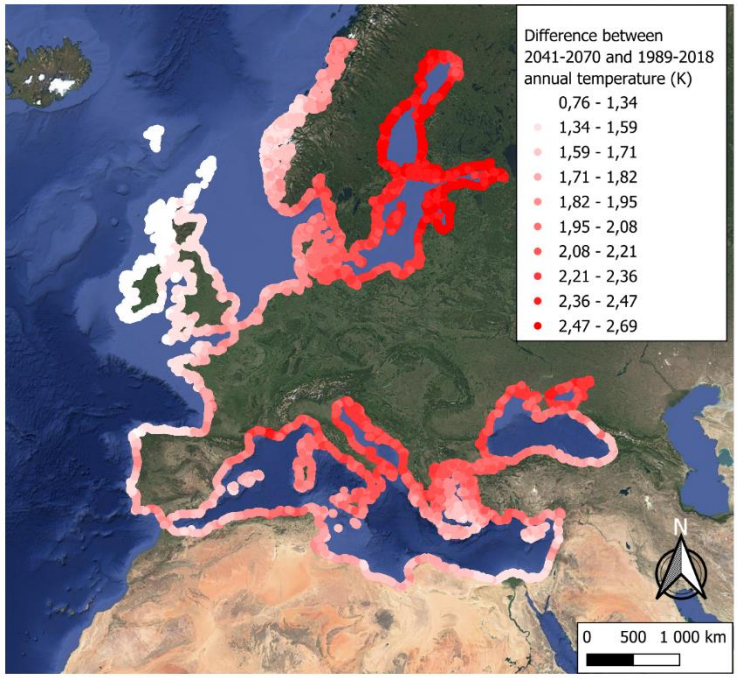

Figure 11. Map of the difference between future annual temperature (2041-2070, SSP3-RCP7) and "present day" values (i.e. difference between CHELSA_tas_2041_2070_ssp370 in DuneFront_D4.1_CHELSA_projections and CHELSA_tas in DuneFront_D4.1_CHELSA_means)

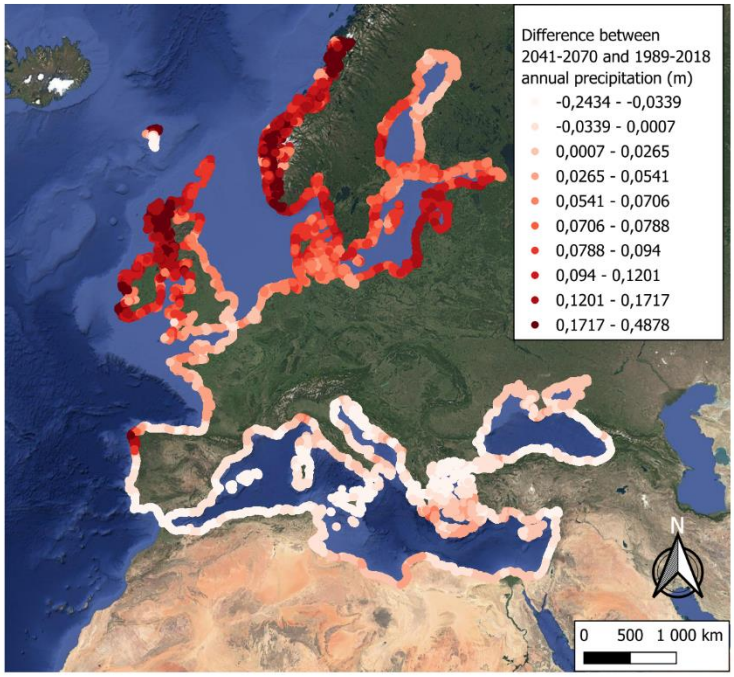

Figure 12. Map of the difference between future annual precipitation (2041-2070, SSP3-RCP7) and "present day" values (i.e. difference between CHELSA_pr_2041_2070_ssp370 in DuneFront_D4.1_CHELSA_projections and CHELSA_pr in DuneFront_D4.1_CHELSA_means)

4.2 Weather layers: Comparison between CHELSA predictions and extrapolations based on recent past trends

We can use CHELSA present-day averages and CHELSA future projections to calculate the annual rates of change implied by CHELSA future projections and compare them to the annual rates of change estimated by linear regression from recent past/current data (i.e. to the layers in DuneFront_D4.1_trends or DuneFront_D4.1_CHELSA_trends). We show Figure 13 an example of this for annual temperature. The absolute difference between the two trends is strongly dependent on the strength of the correlation between time and climate over recent past data (or on the p-value associated with that recent past trend). While the two datasets are in agreement when the Pearson correlation associated with a recent past trend is strong (= when the p-values are low), consistently strong mismatches between that trend and the one expected from CHELSA future projections are very likely where that correlation is weak. While we show only one example here, this qualitative result is robust to whether we use CHELSA or ERA data for the recent past trend, and to the future scenario we choose to compare it to. Importantly, the mismatch between projection-based and recent-past trend estimates can be very high, in some cases on the same order of magnitude as the expected trend. Indeed, the average warming trend implied by CHELSA projections from present day to the 2041-2070 period (for scenario ssp370) is ≈ 0.037 K/year, which is very similar to the mismatch seen at the lowest correlations Figure 13.

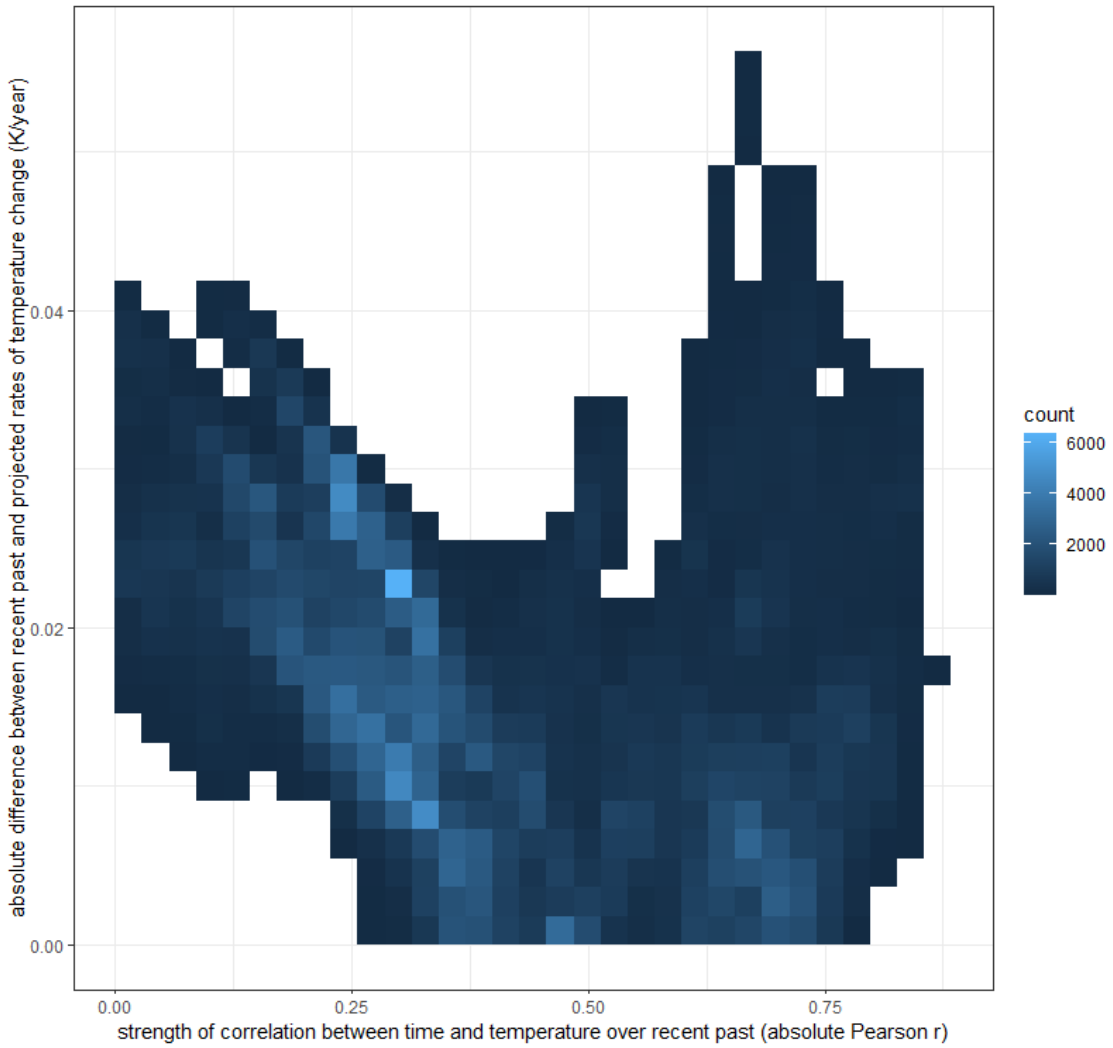

Figure 13. 2D binned plot showing the link between the strength of the recent past temporal trend in annual temperature (absolute r_CHELSA_tas correlation associated with slope_CHELSA_tas in DuneFront_D4.1_CHELSA_trends) and the absolute mismatch between that trend and the one implied from CHELSA future projections (based on ssp370 scenario, using DuneFront_D4.1_CHELSA_means and DuneFront_D4.1_CHELSA_projections to compute annual trends)

Given these potential mismatches, and the fact that the CHELSA projections are informed by multiple climate models and provide predictions over a range of alternative emission scenarios, we recommend that users avoid extrapolating recent past linear trends to infer future weather conditions, or at least do so with extreme caution (e.g. only over short forecast horizons, i.e. years before 2040, and only for transects where the recent past trend is statistically significant). We suggest users utilizing the CHELSA projection(s) most appropriate to their use case instead. We acknowledge that this recommendation cannot be followed for layers where model-informed projections are not available, such as cloud cover or wind

speed. Also, it is important to note that this does not imply that the recent linear trends are "wrong" or have no value; indeed, they should be the layers to choose whenever the intended application is about rates of climate change over the recent past period.

5. Conclusions

This report describes methodology and resulting datasets addressing the physical boundary conditions affecting the effectiveness of Dune-Dike-hybrid (DD-hybrid) Nature-based Solutions (NbS) along the European coastline. Through the collection and processing of high-resolution datasets on coastline features, hydrodynamics, and weather conditions, this work aims to provide a comprehensive understanding of the environmental factors affecting sandy coastlines. The dataset, which spans over 113,000 km of coastline, of which 25,770 km (6.6%) are sandy, provides insight into coastal variability, including the distribution of sandy and eroding shorelines, as well as key hydrodynamic variables like wave height, tidal range, and storm surges. Initial statistical analyses and mapping efforts have revealed significant spatial variability across Europe, with notable differences in coastal dynamics between regions. Future climate projections are also provided under different emission scenarios. These projections indicate significant regional variations, emphasizing the importance of using model-based projections for future conditions rather than relying on recent past trends, which may not accurately reflect future changes.

6. Data availability

All the output layers described in this report are open access and can be freely downloaded from the following Zenodo archive in both geopackage (gpkg) and csv formats, along with a copy of the present report: https://doi.org/10.5281/zenodo.14234693.

- The gpkg files are the reference outputs and should be used preferentially whenever possible, while the csv files are derived from them and provided for additional compatibility and accessibility. Importantly, we advise users dealing with dedicated GIS software (e.g. QGIS) to only use the gpkg files. While csv files can be imported and read by most GIS applications, a few layers/columns contain some missing/NA values (propagated from the raw data, see Section 2.2.2), which can be unrecognized by default import options and cause numerical columns to be mistakenly interpreted as character strings.

For potential access to the underlying "raw" data used in building these layers, many of which are also open, see details Table 1.

7. References

Castelle, B., Kras, E., Masselink, G. et al. (2024): Satellite-derived sandy shoreline trends and interannual variability along the Atlantic coast of Europe. *Scientific Reports*, 14, 13002. https://doi.org/10.1038/s41598-024-63849-4.

Egbert, G.D. and Erofeeva, S.Y. (2002): Efficient inverse modeling of barotropic ocean tides. Journal of Atmospheric and Oceanic Technology, 19.2, 183-204.

Hernández-Cordero, A. I., Gracia Prieto, F. J., Hernández-Calvento, L., Pérez-Chacón Espino, E., Alonso, I. (2015). Proposal for new EU habitats associated with coastal dune fields of the Macaronesian region. A case study in the Canary Islands (Spain). *Journal of Coastal Conservation*, *19*, 213-225. https://doi.org/10.1007/s11852-015-0382-z.

Hersbach, H., Bell, B., Berrisford, P., Biavati, G., Horányi, A., Muñoz Sabater, J., Nicolas, J., Peubey, C., Radu, R., Rozum, I., Schepers, D., Simmons, A., Soci, C., Dee, D., Thépaut, J-N. (2023). ERA5 monthly averaged data on single levels from 1940 to present. Copernicus Climate Change Service (C3S) Climate Data Store (CDS), DOI: 10.24381/cds.f17050d7 (Accessed on 20-05-2024)

Hulskamp R, Luijendijk A, van Maren B, Moreno-Rodenas A, Calkoen F, Kras E, Lhermitte S, Aarninkhof S. (2023). Global distribution and dynamics of muddy coasts. *Nature Communications*, 14, 8259. https://doi.org/10.1038/s41467-023-43819-6.

IPCC, 2023: *Climate Change 2023: Synthesis Report*. Contribution of Working Groups I, II and III to the Sixth Assessment Report of the Intergovernmental Panel on Climate Change [Core Writing Team, H. Lee and J. Romero (eds.)]. IPCC, Geneva, Switzerland, pp. 35-115, doi: 10.59327/IPCC/AR6-9789291691647.

Karger, D.N., Conrad, O., Böhner, J., Kawohl, T., Kreft, H., Soria-Auza, R.W., Zimmermann, N.E., Linder, P., Kessler, M. (2017). Climatologies at high resolution for the Earth land surface areas. *Scientific Data,* 4, 170122. https://doi.org/10.1038/sdata.2017.122

Karger D.N., Conrad, O., Böhner, J., Kawohl, T., Kreft, H., Soria-Auza, R.W., Zimmermann, N.E, Linder, H.P., Kessler, M. (2021): Data from: Climatologies at high resolution for the earth's land surface areas, version 2.1. *EnviDat*. https://doi.org/10.16904/envidat.228.v2.1

Karger, D.N., Schmatz, D., Dettling, G., Zimmermann, N.E. (2019): Data from: High resolution monthly precipitation and temperature timeseries for the period 2006-2100. *EnviDat*. http://dx.doi.org/doi:10.16904/envidat.124.

Karger, D.N., Schmatz, D., Detttling, D., Zimmermann, N.E. (2020): High resolution monthly precipitation and temperature timeseries for the period 2006-2100. *Scientific Data*, 7, 248. https://doi.org/10.1038/s41597-020-00587-y.

Lange, S. (2021): ISIMIP3b bias adjustment fact sheet. https://www.isimip.org/gettingstarted/isimip3b-bias-adjustment/, https://www.isimip.org/documents/413/ISIMIP3b_bias_adjustment_fact_sheet_Gnsz7CO.pdf [accessed 2024-11-22].

Lojek O., Schweiger C., Santos P.R. (2024): Compilation of freely existing socio-economic/administrative boundaries, Version 1.0, DuneFront Project Deliverable 4.3, Technische Universität Braunschweig.

Luijendijk, A., Hagenaars, G., Ranasinghe, R., Baart, F., Donchyts, G., Aarninkhof, S. (2018): The state of the world's beaches. *Scientific Reports*, 8, 6641. https://doi.org/10.1038/s41598-018-24630-6

Muis, S., Apecechea, M.I., Álvarez, J.A., Verlaan, M., Yan, K., Dullaart, J., Aerts, J., Duong, T., Ranasinghe, R., le Bars, D., Haarsma, R., Roberts, M. (2022): Global sea level change indicators from 1950 to 2050 derived from reanalysis and high resolution CMIP6 climate projections. Copernicus Climate Change Service (C3S) Climate Data Store (CDS). DOI: 10.24381/cds.6edf04e0 (Accessed on 10-04-2024)

Riahi, K., Van Vuuren, D. P., Kriegler, E., Edmonds, J., O'neill, B. C., Fujimori, S., (...), Tavoni, M. (2017). The Shared Socioeconomic Pathways and their energy, land use, and greenhouse gas emissions implications: An overview. *Global Environmental Change*, 42, 153-168. https://doi.org/10.1016/j.gloenvcha.2016.05.009